Quasi-boson approximation yields accurate correlation energy in the 2D electron gas

Tobias M. R. Wolf [1] and Chunli Huang [2]
[1]*Department of Physics, University of Texas at Austin, Austin, Texas 78712, USA*
[2]*Department of Physics and Astronomy, University of Kentucky, Lexington, Kentucky 40506-0055, USA*

(Received 3 January 2024; accepted 12 August 2024; published 13 September 2024)

We report the successful adaptation of the quasi-boson approximation, a technique traditionally employed in nuclear physics, to the analysis of the two-dimensional electron gas. We show that the correlation energy estimated from this approximation agrees closely with the results obtained from quantum Monte Carlo simulations. Our methodology comprehensively incorporates the exchange self-energy, direct scattering, and exchange scattering for a particle-hole pair excited out of the mean-field ground state within the equation-of-motion framework. The linearization of the equation of motion leads to a generalized random phase approximation (gRPA) eigenvalue equation whose spectrum indicates that the plasmon dispersion remains unaffected by exchange effects, while the particle-hole continuum experiences a marked upward shift due to the exchange self-energy. Using the gRPA excitation spectrum, we calculate the zero-point energy of the quasi-boson Hamiltonian, thereby approximating the correlation energy of the original Hamiltonian. This research highlights the potential and effectiveness of applying the quasi-boson approximation to the gRPA spectrum, a fundamental technique in nuclear physics, to extended condensed matter systems.

DOI: 10.1103/PhysRevResearch.6.033296

I. INTRODUCTION

The correlation energy, defined as the difference between the exact ground-state energy and the self-consistent Hartree-Fock energy, plays an important role in shaping the phase diagrams of various quantum many-body systems within nuclear and condensed matter physics [1,2]. The success in estimating the correlation energy in nuclear matter for a given nucleon-nucleon interaction profile is largely attributed to the quasi-boson approximation, a method notable for its adaptability and precision. Recent advances have seen this approximation evolve in sophistication and application, as discussed in Ref. [3]. Despite its success in nuclear matter, the quasi-boson approximation has not been extensively applied to metals. This study seeks to bridge this gap by applying the quasi-boson approximation to the two-dimensional electron gas (2DEG) system.

The electron gas model has a long history [4–10], with the first estimation of correlation energy traced back to the random phase approximation (RPA) introduced by Bohm and Pines [9]. The RPA only retains terms in the diagrammatic perturbation series where different Fourier components of the Coulomb interaction V_q are uncoupled. The RPA is an excellent approximation for describing long-distance ($q \to 0$) collective phenomena such as screening since it contains the most diverging geometric series in perturbation theory. However, its efficacy diminishes for short-distance phenomena, where exchange scattering and the particle-particle ladder processes become important. To overcome the limitations of the RPA, an approach often employed introduces the so-called local-field factors into the particle-hole response function [11–14]. This method incorporates short-distance correlations while preserving the original RPA structure, which makes it eminently practical. The first inception of this idea dates back to Hubbard [11], who observed that the exchange contribution of a diagram in the perturbation series will tend to cancel one-half of the direct contribution. He used this insight to approximately evaluate an infinite series of bubble-exchange diagrams and compute the correlation energy. This approach was later refined by Singwi, Tosi, Land and Sjölander (STLS) [12] by using a self-consistent semiclassical approximation for the local-field factors. More recently, similar ideas have been studied in the context of density functional theory as exact-exchange-kernel (or RPAx) methods [15,16]. Currently, the quantum Monte Carlo [14,17,18] calculation is recognized as providing the most accurate estimation of correlation energy, setting a benchmark for comparison in this field.

In this study, we adopt an equation of motion approach to numerically sum over the complete geometric series of bubble-exchange diagrams, thereby obtaining the particle-hole excitation spectrum. Subsequently, we leverage this spectrum to compute the correlation energy. This computation is based on the assumption that the commutator of the particle-hole annihilation operator (b_{ni}) and the particle-hole creation operator ($b^\dagger_{mj}$) can be replaced by its Hartree-Fock (HF) expectation value, i.e.,

$$[b_{ni}, b^\dagger_{mj}] \approx \langle \mathrm{HF}|[b_{ni}, b^\dagger_{mj}]|\mathrm{HF}\rangle = \delta_{mn}\delta_{ij}, \tag{1}$$

where m, n (i, j) label particle (hole) states and $|\mathrm{HF}\rangle$ is the Hartree-Fock ground state. This is known as the quasi-boson

Published by the American Physical Society under the terms of the Creative Commons Attribution 4.0 International license. Further distribution of this work must maintain attribution to the author(s) and the published article's title, journal citation, and DOI.

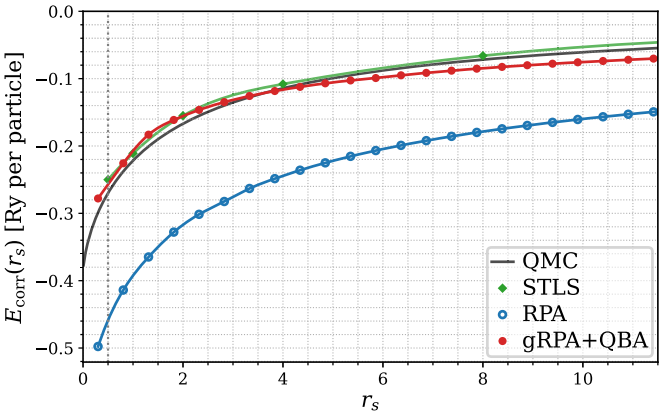

FIG. 1. Correlation energy vs electron gas parameter r_s in the 2DEG obtained in the QBA for the generalized RPA spectrum. The quasi-boson approximation yields results in good agreement with the QMC and the local-field method (STLS) over a wide range of r_s. The QMC fit and STLS data are from Refs. [17] and [13], respectively. For QBA, we used a Yukawa screening wave vector of $\kappa = 0.1dk$, where dk is the discretization.

approximation (QBA) because the above equation would have been exact if b_{ni} and $b^\dagger_{mj}$ truly were bosonic operators. Our results demonstrate that the correlation energy calculated within the QBA is in good agreement with quantum Monte Carlo (QMC) results, as shown in Fig. 1. This intriguing finding suggests that while the exact 2DEG ground state $|0\rangle$ is surely orthogonal to the Hartree-Fock ground state, $\langle 0|\mathrm{HF}\rangle \approx 0$, the expectation value of the above commutator is well approximated by its HF value,

$$\langle 0|[b_{ni}, b^\dagger_{mj}]|0\rangle \approx \langle \mathrm{HF}|[b_{ni}, b^\dagger_{mj}]|\mathrm{HF}\rangle. \tag{2}$$

In terms of the many-body wave function, the QBA introduces *zero-point* quantum fluctuation into the HF ground state [19]. While the QBA is a widely used method in nuclear many-body physics [3,20,21], it remains largely uncharted in condensed matter physics, likely due to its computational complexities.

This paper is structured as follows: Sec. II revisits the application of the equation of motion to derive the generalized RPA equation. We then numerically solve this equation to obtain the excitation eigenspectrum and response functions of the electron gas across varying density parameters r_s. We discuss the impact of exchange self-energy and exchange scattering on the plasmon dispersion and particle-hole continuum. In Sec. III, we employ a quasi-boson approximation to obtain the 2DEG correlation energy as the ground-state energy of a bosonic Hamiltonian for residual interactions. Making use of the gRPA eigenspectrum then allows us to evaluate the quasi-boson correlation energy at different r_s. We conclude with a discussion and outlook in Sec. IV.

II. EQUATION OF MOTION APPROACH

In this section, we use the equation of motion approach to derive the generalized random phase approximation (gRPA) eigenvalue equation and compute the excitation spectrum associated with the creation of a single particle-hole pair in 2DEG. To remind the reader, the 2DEG Hamiltonian in momentum space is

$$H = \sum_{k\sigma} \epsilon_k \, c^\dagger_{k\sigma} c_{k\sigma} + \frac{1}{2} \sum_{q\neq 0} V_q \; :\rho_q \rho_{-q}:, \tag{3}$$

where $\epsilon_k = \hbar^2 k^2/2m$ is the dispersion, $c^{(\dagger)}_{k\sigma}$ destroys (creates) an electron with spin σ and momentum k, $\rho_q = \sum_{k\sigma} c^\dagger_{k+q\sigma} c_{k\sigma}$ is the density operator, $V_q = 2\pi e^2/A\sqrt{q^2+\kappa^2}$ is the Fourier component of (screened) Coulomb potential, and $:\cdot:$ denotes normal ordering with respect to the vacuum state. A is the area of the 2DEG and $\kappa \simeq 0.1dk$ is the Thomas-Fermi cutoff parameter, which we choose to be small compared to our momentum discretization dk to recover the long-range limit [22]. Expressing Eq. (3) in units of effective Bohr radius $a_B = \hbar^2/(me^2)$ and Rydberg energy $\mathrm{Ry} = e^2/(2a_B)$ allows to parametrize the 2DEG by the dimensionless Wigner-Seitz radius $r_s\, a_B = (\pi\, n)^{-1/2}$. The latter can be interpreted as the average distance between electrons given the electronic density n. For high densities ($r_s \quad 0$) the kinetic term dominates, while at low densities ($r_s \quad \infty$) Coulomb interactions will take over. In the Hartree-Fock approximation, the ground state is a Slater determinant state $|\mathrm{HF}\rangle$ of plane waves and the quasiparticle has the energy dispersion

$$\epsilon^{\rm HF}_k = \epsilon_k + \Sigma^F_k, \tag{4}$$

where $\Sigma^F_k = -\sum_{|k'|<k_F} V_{k-k'}$ is the exchange self-energy.

A. Generalized RPA and time-dependent mean field

Given the many-body ground state $|0\rangle$, we consider charge-neutral excitations $|\nu q\rangle = Q^\dagger_{\nu q}|0\rangle$ with momentum q created by operators

$$Q^\dagger_{\nu q} = \sum_{k\in K^+_q} (X_{\nu q})_k c^\dagger_{k+q} c_k - \sum_{k\in K^-_q} (Y_{\nu q})_k c^\dagger_k c_{k-q}. \tag{5}$$

The summations account for all particle-hole pairs consistent with the Pauli-exclusion principle, described by $K^\pm_q = \{k \,|\, \epsilon_k < \epsilon_F < \epsilon_{k\pm q}\}$. The number of pairs, $M_q = |K^\pm_q|$, is finite due to discretization. The first term in Eq. (5) creates a particle-hole pair with momentum $+q$ since $|k| < k_F$, $|k+q| > k_F$. The second term annihilates a particle-hole pair with momentum since $|k| < k_F$, $|k-q| > k_F$. Here and in what follows, holes are labeled with momentum k, k' and particles are labeled with $k \pm q$ and $k' \pm q$. The spin index is being summed over and hence omitted [23].

The Hartree-Fock state $|\mathrm{HF}\rangle$ is the vacuum of the annihilation operator $Q_{\nu q}|\mathrm{HF}\rangle = 0$ only when $Y = 0$. The many-body state annulled by $Q_{\nu q}$ when $Y \neq 0$ is sometimes called the gRPA state,

$$Q_{\nu q}|0\rangle = 0. \tag{6}$$

In contrast to state $|\mathrm{HF}\rangle$, which is void of any particle-hole pairs, a state satisfying Eq. (6) must inherently incorporate such pairs, resulting in a better approximation to the ground state.

The amplitudes $X_{\nu q}$, $Y_{\nu q}$ have to satisfy the many-body Schrödinger equation

$$[H, Q^\dagger_{\nu q}]\,|0\rangle = \hbar \;\; _{\nu q} Q^\dagger_{\nu q}\,|0\rangle\,, \tag{7}$$

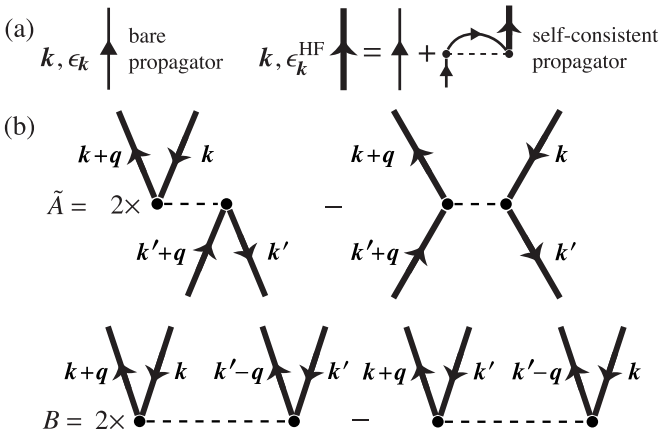

FIG. 2. Diagrammatic interpretation for the matrix elements of A, B in the excitation eigenequation for the 2DEG [cf. Eq. (9a)]. (a) Bare noninteracting propagator and self-consistent propagator accounting for Fock self-energy renormalization. (b) TDHF matrix elements with direct and exchange contributions to the scattering ($\tilde{A}$) and to the double-excitations (B). Note that for A, we only show the contributions $\tilde{A}$ without the trivial kinetic term. Spin summation leads to factors of 2 in the direct diagrams.

where $\hbar\ _{\nu\boldsymbol{q}}$ is the excitation energy. The formidable task of solving Eq. (7) becomes possible using Eq. (5), the vacuum condition (6), and the quasi-boson approximation [3,20]. We multiply Eq. (7) from the left with $Q_{\nu\boldsymbol{q}}$ and use Eq. (6) to find the scalar equation

$$\langle 0|\,[Q_{\nu\boldsymbol{q}},[H,Q^\dagger_{\nu\boldsymbol{q}}]]\,|0\rangle = \hbar\ _{\nu\boldsymbol{q}}\,\langle 0|\,[Q_{\nu\boldsymbol{q}},Q^\dagger_{\nu\boldsymbol{q}}]\,|0\rangle\,. \tag{8}$$

We now use the quasi-boson approximation [3,20] to evaluate the commutator expectation values in Eq. (8) by replacing $|0\rangle$ with the Hartree-Fock state $|\mathrm{HF}\rangle$. We emphasize that this substitution does not suggest that $|\mathrm{HF}\rangle$ closely approximates $|0\rangle$, but merely reflects the similarity of specific *correlator expectation values*. With this approximation, Eq. (8) leads to the gRPA eigenvalue equation [3,20,24]

$$\sum_{\boldsymbol{k}}[\quad _{\boldsymbol{q}}]_{\boldsymbol{k}',\boldsymbol{k}}\begin{bmatrix}X_{\nu\boldsymbol{q}}\\ Y_{\nu\boldsymbol{q}}\end{bmatrix}_{\boldsymbol{k}} = \hbar\ _{\nu\boldsymbol{q}}\begin{bmatrix}1 & 0\\ 0 & -1\end{bmatrix}\begin{bmatrix}X_{\nu\boldsymbol{q}}\\ Y_{\nu\boldsymbol{q}}\end{bmatrix}_{\boldsymbol{k}'}, \tag{9a}$$

where the matrix elements of the matrix $_{\boldsymbol{q}}$ are given by

$$[\quad _{\boldsymbol{q}}]_{\boldsymbol{k}',\boldsymbol{k}} = \begin{bmatrix}A_{\boldsymbol{k}'+\boldsymbol{q},\boldsymbol{k};\boldsymbol{k}+\boldsymbol{q},\boldsymbol{k}} & B_{\boldsymbol{k}'+\boldsymbol{q},\boldsymbol{k};\boldsymbol{k}-\boldsymbol{q},\boldsymbol{k}}\\ (B_{\boldsymbol{k}'-\boldsymbol{q},\boldsymbol{k};\boldsymbol{k}+\boldsymbol{q},\boldsymbol{k}})^* & (A_{\boldsymbol{k}'-\boldsymbol{q},\boldsymbol{k};\boldsymbol{k}-\boldsymbol{q},\boldsymbol{k}})^*\end{bmatrix} \tag{9b}$$

with

$$\begin{aligned}A_{\boldsymbol{k}'+\boldsymbol{q},\boldsymbol{k};\boldsymbol{k}+\boldsymbol{q},\boldsymbol{k}} &= \left(\epsilon_{\boldsymbol{k}+\boldsymbol{q}}+\Sigma^F_{\boldsymbol{k}+\boldsymbol{q}}-\epsilon_{\boldsymbol{k}}-\Sigma^F_{\boldsymbol{k}}\right)\delta_{\boldsymbol{k},\boldsymbol{k}'}+2V_{\boldsymbol{q}}-V_{\boldsymbol{k}-\boldsymbol{k}'},\\ B_{\boldsymbol{k}'+\boldsymbol{q},\boldsymbol{k};\boldsymbol{k}-\boldsymbol{q},\boldsymbol{k}} &= 2V_{\boldsymbol{q}}-V_{\boldsymbol{k}-(\boldsymbol{k}'-\boldsymbol{q})}.\end{aligned} \tag{9c}$$

In Sec. III below, we see that Eqs. (8) and (9a) have the same form as the equations of motion of a bosonic Hamiltonian.

For a specific $\boldsymbol{q}$, Eq. (9a) represents a $2M_{\boldsymbol{q}}\times 2M_{\boldsymbol{q}}$ eigenvalue problem, where $M_{\boldsymbol{q}}$ denotes the number of points in the set $K^+_{\boldsymbol{q}}$ (or $K^-_{\boldsymbol{q}}$). The matrix elements of $_{\boldsymbol{q}}$ represent various scattering amplitudes for the mean-field quasiparticles, shown as Feynman diagrams in Fig. 2. The matrix $_{\boldsymbol{q}}$ captures both the direct and the exchange scattering between particle-hole pairs with momentum $+\boldsymbol{q}$ and $-\boldsymbol{q}$. Matrix A characterizes the scattering between two pairs in $K^+_{\boldsymbol{q}}$ or two pairs in $K^-_{\boldsymbol{q}}$. Conversely, matrix B describes the scattering involving one particle-hole pair from $K^+_{\boldsymbol{q}}$ and another from $K^-_{\boldsymbol{q}}$. The simplicity and similarity of matrix elements in A and B result from the fact that the Hartree-Fock quasiparticles in the 2DEG are just plane wave states. In systems with additional orbital degrees of freedom, form factors would enter the matrix elements.

The entirety of the eigenspectrum of Eq. (9a) provides the basis for constructing the spectral representation of the particle-hole Green function [1]. This foundation allows us to express the density-density response function as

$$\chi(\boldsymbol{q},\ \ ) = \sum_{\nu=-M_{\boldsymbol{q}}}^{M_{\boldsymbol{q}}}\mathrm{sgn}(\ _{\nu\boldsymbol{q}})\frac{R_{\nu\boldsymbol{q}}}{-\ _{\nu\boldsymbol{q}}+i0^+}. \tag{10}$$

Here, $R_{\nu\boldsymbol{q}}$ represents the modulus squared of the sum of all entries of a gRPA eigenvector, defined as

$$R_{\nu\boldsymbol{q}} \equiv |\langle\nu\boldsymbol{q}|\rho_{\boldsymbol{q}}|0\rangle|^2 = \frac{1}{A}\left|\sum_{\boldsymbol{k}=1}^{M_{\boldsymbol{q}}}(X_{\nu\boldsymbol{q}})_{\boldsymbol{k}}+(Y_{\nu\boldsymbol{q}})_{\boldsymbol{k}}\right|^2, \tag{11}$$

which is the probability of finding one quanta of density excitation in the excited state $|\nu\boldsymbol{q}\rangle$. In this notation, $R_{\nu\boldsymbol{q}}$ is proportional to the residue of $\chi(\boldsymbol{q},\ \ )$ at its simple pole $_{\nu}(\boldsymbol{q})$, serving as a metric for measuring the collectivity of a particular gRPA eigenvector. Particularly in cases where the excitation is an equal superposition of all particle-hole pairs, such as when $(X_{\nu\boldsymbol{q}})_{\boldsymbol{k}}+(Y_{\nu\boldsymbol{q}})_{\boldsymbol{k}}=1/M_{\boldsymbol{q}}$, $R_{\nu\boldsymbol{q}}$ peaks at unity. Thus, $R_{\nu\boldsymbol{q}}$ allows to distinguish between collective excitations and uncorrelated particle-hole pair excitations, especially when the former merges into the particle-hole continuum.

B. Results: Charge-neutral excitation spectrum and density-density response

In this subsection, we designate the eigenvalue spectrum derived from Eq. (9a) as the TDHF approximation and proceed to compare it with two other prevalent approximations. The first of these is the TDH approximation, which involves setting both the exchange self-energy and exchange-scattering to zero, i.e., $\Sigma^F_{\boldsymbol{k}}=V_{\boldsymbol{k},\boldsymbol{k}}=V_{\boldsymbol{k},\boldsymbol{k}-\boldsymbol{q}}=0$ in Eq. (9c). This approach is equivalent to the RPA approximation introduced by Bohm and Pines. The second approach, denoted TDH* approximation, differs slightly; here, we retain the exchange self-energy while setting the exchange scattering to zero, i.e., $\Sigma^F_{\boldsymbol{k}}\neq 0, V_{\boldsymbol{k},\boldsymbol{k}}=V_{\boldsymbol{k},\boldsymbol{k}-\boldsymbol{q}}=0$ in Eq. (9c). Note that both the TDHF and TDH are classified as conserving approximations, following Baym's criteria [25], whereas the TDH* is not.

Figures 3(a) and 3(b) present the excitation spectrum computed using the TDH approximation for $r_s=1$ and $r_s=4$, respectively. This spectrum consists of a continuum of particle-hole excitations, which exhibit small $R_{\nu\boldsymbol{q}}$ values, and one plasmon mode characterized by significantly large $R_{\nu\boldsymbol{q}}$ values. As r_s increases, the plasmon mode progressively merges into the continuum at larger q.

Figures 3(c) and 3(d) depict the excitation spectrum determined within the TDHF approximation for $r_s=1$ and $r_s=4$. Notably, the plasmon mode is fully merged into the particle-hole continuum. Moreover, the near-zero-frequency excitations near $2k_F$ exhibit an enhanced $R_{\nu\boldsymbol{q}}$. A deeper insight

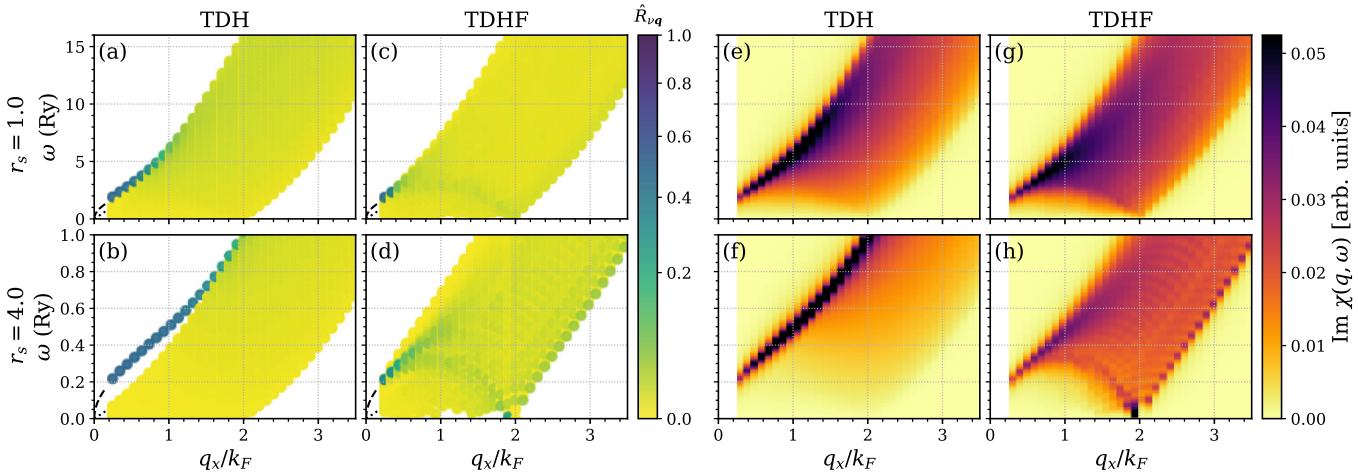

FIG. 3. Spectrum, plasmon dispersion, and many-body stability of the 2DEG. (a)–(d) Excitation spectra, over an extended range of q including $2k_F$, obtained using the gRPA equations [cf. Eq. (9a)] for time-dependent Hartree (TDH) and time-dependent Hartree-Fock with exchange self-energy (TDHF). The color is the normalized density response residue $\hat{R}_{\nu q} = R_{\nu q}/\sum_\nu R_{\nu q}$ [cf. Eq. (11)]. (e)–(h) The corresponding charge susceptibilities for each scheme. Results are presented for electron gas density parameters $r_s = 1.0, 4.0$. Notably, in the expanded q range, TDHF shows a tendency to forming charge-density waves, see main text. Here, we used $dk = 0.08k_F$, $\kappa = 0.15dk$, and $q \quad 3dk$.

into these effects can be obtained by analyzing the spectral weight of the density fluctuations in Fig. 3(h). In the TDH approximation, the spectral weight is concentrated around the plasmon mode. This concentration becomes more pronounced with increasing r_s due to the larger energy separation between the particle-hole continuum and the plasmon mode. Conversely, in the TDHF approximation, the spectral weight is more uniformly spread across the continuum. A notable peak in spectral weight is observed at wave number $q = 2k_F$. This mode represents an inherent instability of the electron gas toward the formation of a charge (or spin) density wave [15,26,27]. As r_s increases, this mode gains more spectral weight and moves closer to zero energy. When this mode attains zero energy, we have to consider the charge-density wave as competing ground state, and subsequently, examine the excitation spectrum based on this state. The inclusion of screening in our long-range Coulomb interaction, controlled by κ, suppresses the charge-density wave instability. For a discussion on how the screening constant curbs the density wave instability in a three-dimensional electron gas, see Ref. [28].

In Fig. 4, we focus on the small q region of the particle-hole excitation spectrum. We use dashed lines to indicate the classical plasmon-dispersion

$$\hbar \quad _{\rm pl}(q) = \frac{2\sqrt{2qa_B}}{r_s} \text{ Ry}, \tag{12}$$

and the maximum of the particle-hole continuum given by the parabolic dispersion, i.e.,

$$\max(\epsilon_{\boldsymbol{k}+\boldsymbol{q}} - \epsilon_{\boldsymbol{k}}) = (2k_F q + q^2)a_B^2 \text{ Ry}. \tag{13}$$

Figures 4(a) and 4(b) demonstrate that the TDH approximation closely aligns with Eqs. (12) and (13). There is an extensive q range where the plasmon mode is spectrally isolated from the uncorrelated particle-hole spectrum. Figures 4(c) and 4(d) show the spectrum obtained in the TDHF approximation. While the plasmon dispersion remains aptly described by Eq. (12), the boundary of the particle-hole continuum shifts notably up compared to Eq. (13). The upward shift of the particle-hole continuum boundary arises because the exchange self-energy of the holes (i.e., occupied states) are more negative than that of the particle state (i.e., unoccupied state). Consequently, within the specified q range in Fig. 4, the plasmon mode undergoes Landau damping. To provide a contrasting perspective, Figs. 4(e) and 4(f) show the excitation spectra for TDH*. As discussed above, TDH* is not a conserving approximation: the exchange effect is only retained in the single-particle propagator but omitted in the vertices [25]. While it describes the particle-hole continuum effectively, it inadequately captures the plasmon mode dispersion.

Figures 4(g)–4(l) show the spectral function Im$\chi(q, \quad)$ of the density response computed with different approximation schemes. The most important feature in these plots is that the spectral weight is almost completely exhausted by the plasmon dispersion at small q. This characteristic persists even when the plasmon dispersion slightly overlaps with the continuum, as shown in Fig. 4(d). This observation signals the validity for a powerful approximation that effectively describes the long-wavelength limit of the dynamical structure factor in the electron liquid. The method is known as "single-mode approximation" such that Im$\chi(q, \quad)/\pi \sim f(q)\delta[\quad - \quad _{\rm pl}(q)]$.

In Fig. 5, we show the dynamic and spatial correlation function Re$\chi(q, \quad)$ in different approximation schemes for two density parameters r_s. In all cases, the response undergoes a sign change near the (renormalized) plasmon pole and has finite momenta and frequency regions where retarded screened interactions can be attractive. At moderate density parameter $r_s = 1$ the approximations yield comparable correlation functions, while at the smaller density ($r_s = 4$) the Reχ is enhanced near smaller frequencies and $2k_F$ due to exchange scattering. Furthermore, in the TDHF approximation, the sign change is shifted toward lower frequencies and broadened

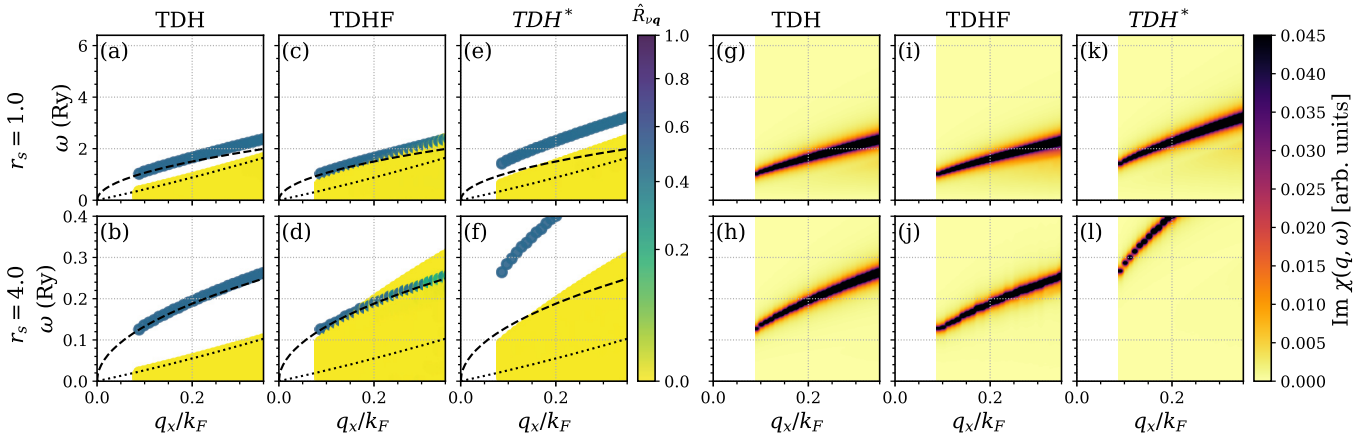

FIG. 4. Long-wavelength spectrum and plasmon modes of the 2DEG. (a)–(f) Excitation spectra obtained as eigensolutions of the gRPA equations [cf. Eq. (9a)] for three different approximation schemes: TDH, TDHF, and time-dependent Hartree with exchange self-energy (TDH*). The color is the normalized density response residue $\hat{R}_{\nu q} = R_{\nu q}/\sum_\nu R_{\nu q}$ [cf. Eq. (11)]. (g)–(l) The corresponding charge susceptibilities for each scheme. All results are plotted for two electron gas density parameters, $r_s = 1.0, 4.0$, as indicated to the left of each row. Color intensities in the spectra and susceptibilities represent the magnitude of the spectral weight $\hat{R}_\nu(q)$ and the imaginary part of the charge susceptibility $\chi(q, \quad)$, respectively. The plasmon modes for TDH and TDHF are comparable as a result of a conserving approximation. Note that TDH* gives unphysical results, see main text. Here, we used $dk = 0.03k_F$, $\kappa = 0.15dk$, and $q \quad 3dk$.

where the plasmon mode merged into the particle-hole continuum [cf. Figs. 3(h) and 5]. These observations highlight the importance of taking into account exchange contributions to correlation functions and effective screened interactions, already at density parameters $r_s \sim 4$.

III. QUASI-BOSON APPROXIMATION AND CORRELATION ENERGY

In this section, we use the gRPA eigenvalue spectrum in Sec. II to compute the correlation energy using a quasi-boson approximation. To begin, let us revisit some fundamental properties of the bosonic quadratic Hamiltonian

$$K = Ab^\dagger b + \tfrac{1}{2}(Bb^\dagger b^\dagger + B^* bb), \tag{14}$$

where A and B are parameters, and $b^\dagger$ and b are bosonic creation and annihilation operators. Due to its quadratic nature,

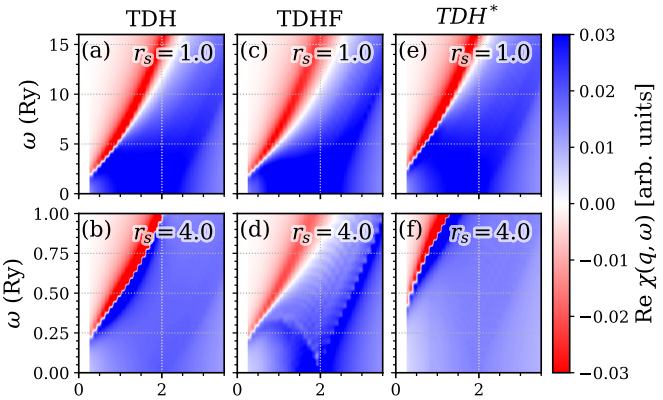

FIG. 5. Comparison of the correlation function Re$\chi(q, \quad)$ for momenta q and real frequencies of the 2DEG at density parameters $r_s = 1.0$ (top) and $r_s = 4$ (bottom) and different approximation schemes: (a) and (b) TDH, (c) and (d) TDHF, and (e) and (f) TDH*. Here, we used $dk = 0.08k_F$, $\kappa = 0.15dk$, and $q \quad 3dk$.

the double commutator of K with the creation and annihilation operators yields *scalars* instead of operators. To transform K into the diagonal form $K = \quad Q^\dagger Q$, where $[Q, Q^\dagger] = 1$, we define $Q^\dagger = Xb^\dagger - Yb$ and evaluate its double commutator with K,

$$\begin{aligned}
&[Q, [K, Q^\dagger]] \\
&\quad = [X^* \quad Y^*]\begin{bmatrix} [b, [K, b^\dagger]] & -[b, [K, b]] \\ -[b^\dagger, [K, b^\dagger]] & [b^\dagger, [K, b]] \end{bmatrix}\begin{bmatrix} X \\ Y \end{bmatrix} \\
&\quad = [X^* \quad Y^*]\begin{bmatrix} A & B \\ B^* & A \end{bmatrix}\begin{bmatrix} X \\ Y \end{bmatrix} = \quad .
\end{aligned} \tag{15}$$

Using $|X|^2 - |Y|^2 = 1$, Eq. (15) leads to the eigenvalue equation

$$\begin{bmatrix} A & B \\ B^* & A \end{bmatrix}\begin{bmatrix} X \\ Y \end{bmatrix} = \begin{bmatrix} 1 & 0 \\ 0 & -1 \end{bmatrix}\begin{bmatrix} X \\ Y \end{bmatrix}, \tag{16}$$

which has the same structure as gRPA equation (9a).

Next, we implement the quasi-boson approximation Eq. (1) by assuming that the fermion bilinears $b_{k+q,k} \equiv c^\dagger_k c_{k+q}$ satisfy the bosonic commutation relation $[b_{k+q,k}, b^\dagger_{k'+q,k'}] \approx \delta_{k,k'}$. A bosonic Hamiltonian, denoted as H_B, is then constructed by equating the double commutators of H_B with the quasi-boson creation and annihilation operators to the matrix elements of the gRPA equation, i.e.,

$$[b_{k'+q,k'}, [H_B, b^\dagger_{k+q,k}]] = A_{k'+q,k\,;k+q,k}, \tag{17a}$$

$$[b^\dagger_{k'+q,k'}, [H_B, b^\dagger_{k-q,k}]] = -B_{k'+q,k\,;k-q,k}. \tag{17b}$$

Analogous to the example in the beginning of this section, see Eqs. (14)–(16), we find

$$\begin{aligned}
H_B = \sum_{q,k,k'} \Big(& A_{k'+q,k\,;k+q,k}\, b^\dagger_{k'+q,k}\, b_{k+q,k} \\
& + \frac{1}{2} B_{k'+q,k\,;k-q,k}\, b^\dagger_{k'+q,k}\, b^\dagger_{k-q,k} + \text{c.c.} \Big)
\end{aligned}$$

$$= \frac{1}{2}\sum_{\boldsymbol{k},k\ ,\boldsymbol{q}} [b^{\dagger}_{\boldsymbol{k}\ +\boldsymbol{q},\boldsymbol{k}}\, b_{\boldsymbol{k}\ -\boldsymbol{q},\boldsymbol{k}'}][\quad\ \ _{\boldsymbol{q}}]_{\boldsymbol{k}\ ,\boldsymbol{k}} \begin{matrix} b_{\boldsymbol{k}+\boldsymbol{q},\boldsymbol{k}} \\ b^{\dagger}_{\boldsymbol{k}-\boldsymbol{q},\boldsymbol{k}} \end{matrix}\Bigg] - \frac{1}{2}\mathrm{tr}\, A, \tag{18}$$

where we used $b^{\dagger}b = \frac{1}{2}(b^{\dagger}b + bb^{\dagger} - 1)$ and $\ _{\boldsymbol{q}}$ from gRPA equation (9a). Leveraging the eigenvalue spectrum leads to

$$\begin{aligned} H_B &= \frac{1}{2}\sum_{\boldsymbol{q}}\sum_{\nu=1}^{M_{\boldsymbol{q}}} \hbar\ \ _{\nu\boldsymbol{q}}[Q^{\dagger}_{\nu\boldsymbol{q}}Q_{\nu\boldsymbol{q}} + Q_{\nu\boldsymbol{q}}Q^{\dagger}_{\nu\boldsymbol{q}}] - \frac{\mathrm{tr}\, A}{2} \\ &= \frac{1}{2}\sum_{\boldsymbol{q}}\sum_{\nu=1}^{M_{\boldsymbol{q}}} \hbar\ \ _{\nu\boldsymbol{q}}Q^{\dagger}_{\nu\boldsymbol{q}}Q_{\nu\boldsymbol{q}} + E_{\mathrm{zp}}, \end{aligned} \tag{19}$$

where $Q^{\dagger}_{\nu\boldsymbol{q}}$ is defined in Eq. (5). Here, $\nu = 1, \ldots, M_{\boldsymbol{q}}$ labels the positive eigenvalues. The Hamiltonian H_B describes a portion of the residual interaction within mean-field theory as a collection of harmonic oscillators and the zero-point energy E_{zp}. A similar bosonic Hamiltonian can be derived using a path-integral approach, as detailed in Chap. 4 of Ref. [29]. The ground-state energy of H_B is

$$E_{\mathrm{zp}} = \frac{1}{2}\sum_{\boldsymbol{q}}\sum_{\nu=1}^{M_{\boldsymbol{q}}} \hbar\ \ _{\nu\boldsymbol{q}} - \frac{1}{2}\sum_{\boldsymbol{k},\boldsymbol{q}} A_{\boldsymbol{k}+\boldsymbol{q},\boldsymbol{k};\boldsymbol{k}+\boldsymbol{q},\boldsymbol{k}}. \tag{20}$$

In Fig. 1, we show the total correlation energy per particle $E_{\mathrm{corr}} = E_{\mathrm{zp}}/N$ at different r_s, where $N = n_e A$ is the number of electrons. Our results show good agreement with those obtained from QMC studies as well as the STLS approximation. We note that our correlation energy calculation is formally equivalent to a series of ring-exchange diagrams, and is thus inherently free from log divergences as they would appear in a truncated perturbative expansion. The TDH approximation discussed in Sec. II B is mathematically equivalent to a series of ring diagrams [7,9].

IV. DISCUSSION AND OUTLOOK

To summarize, we have studied the charge-neutral particle-hole excitation spectrum and response function of the 2DEG by formulating the generalized RPA eigenvalue equation for extended systems. We used the resulting excitation spectrum to evaluate the 2DEG correlation energy by invoking the quasi-boson approximation. The gRPA and QBA method presented in this work has a convenient diagrammatic construction and systematically accounts for both direct scattering and exchange scattering (i.e., TDH and TDHF).

In stark contrast, the most commonly used RPA method based on coupling constant integration is exclusively a TDH method [4], i.e., it does not account for exchange effects. In that method, the susceptibility simplifies to $\chi_\lambda(\boldsymbol{q},\ \ ) = \chi_0(\boldsymbol{q},\ \ )/[1 - \lambda V_{\boldsymbol{q}}\chi_0(\boldsymbol{q},\ \ )]$, where χ_0 is the noninteracting susceptibility and λ the coupling constant. The correlation energy E_{corr} is given analytically through coupling-constant integration involving $\chi_\lambda(\boldsymbol{q}, i\ \ )$. While such a momentum-local RPA approximation is powerful for analytical studies, it (1) is only strictly valid at high densities ($r_s \ll 1$) and (2) can only be extended to include exchange effects by introducing semiclassical self-consistent local-field factors [12,13] or exchange kernel approximations [15,16]. Such local-field methods are not easily applied to multiorbital systems and their validity is not easily checked. While more recent exchange kernel methods can reproduce TDHF response functions to leading order, they typically still require systematic kernel approximations. Our gRPA and QBA method has none of these limitations. However, our method requires careful diagrammatic construction, choice of discretization, particle-hole basis truncation, and large-scale numerical diagonalization. As we showed in this work, these issues can be overcome, leading to results that rival STLS and QMC methods. Further controlled improvements of the gRPA + QBA method presented here are possible through self-consistent RPA, see Ref. [3]. In this extension, ground-state correlations are taken into account when evaluating expectation values in Eq. (8). This strategy significantly increases the computational cost, but could allow to study cases when correlations are exceptionally strong and minimizes the Pauli principle violation implied by the bosonization.

Recent discoveries of correlated states and superconductivity in multilayer graphene [30–32] and Wigner crystals in TMDs [33–38] provide strong motivation to study gRPA correlation effects in these materials. In particular, this may allow to understand why their mean-field descriptions tend to have some systematic issues. In this context, we highlight that the formalism in this work straightforwardly generalizes to multicomponent 2DEG-like problems, such as spin, valley, and sublattice in the continuum models of graphene and TMD multilayers. It also generalizes to other types of particle-hole excitation spectra and response functions, including those for spin- and valley-flip excitations.

To conclude, this work opens exciting possibilities by providing a practical way to explore and understand correlations in complex two-dimensional condensed matter systems.

ACKNOWLEDGMENTS

T.M.R.W. is grateful for the financial support from the Swiss National Science Foundation (Postdoc. Mobility Grant No. 203152) and for the hospitality of the University of Kentucky, where part of this work was done. This research was partially supported by the National Science Foundation through the Center for Dynamics and Control of Materials (Grant No. DMR-2308817).

[1] D. J. Thouless, *The Quantum Mechanics of Many-Body Systems* (Courier Corporation, Chelmsford, 2014).

[2] D. J. Rowe, *Nuclear Collective Motion: Models and Theory* (World Scientific, Singapore, 2010).

[3] P. Schuck, D. Delion, J. Dukelsky, M. Jemai, E. Litvinova, G. Röpke, and M. Tohyama, Equation of motion method for strongly correlated Fermi systems and extended RPA approaches, Phys. Rep. **929**, 1 (2021).

[4] G. Giuliani and G. Vignale, *Quantum Theory of the Electron Liquid* (Cambridge University, Cambridge, 2005).

[5] D. Pines and P. Nozieres, *The Theory of Quantum Liquids* (Addison-Wesley, Reading, 1990).

[6] C. Herring, *Magnetism: Exchange Interactions among Itinerant Electrons* (Academic, New York, 1966).

[7] M. Gell-Mann and K. A. Brueckner, Correlation energy of an electron gas at high density, Phys. Rev. **106**, 364 (1957).

[8] P. Nozieres and D. Pines, Correlation energy of a free electron gas, Phys. Rev. **111**, 442 (1958).

[9] D. Bohm and D. Pines, A collective description of electron interactions: III. Coulomb interactions in a degenerate electron gas, Phys. Rev. **92**, 609 (1953).

[10] A. Rajagopal and J. C. Kimball, Correlations in a two-dimensional electron system, Phys. Rev. B **15**, 2819 (1977).

[11] J. Hubbard, The description of collective motions in terms of many-body perturbation theory. II. The correlation energy of a free-electron gas, Proc. R. Soc. London A **243**, 336 (1958).

[12] K. Singwi, M. Tosi, R. Land, and A. Sjölander, Electron correlations at metallic densities, Phys. Rev. **176**, 589 (1968).

[13] M. Jonson, Electron correlations in inversion layers, J. Phys. C **9**, 3055 (1976).

[14] H.-J. Schulze, P. Schuck, and N. Van Giai, Two-dimensional electron gas in the random-phase approximation with exchange and self-energy corrections, Phys. Rev. B **61**, 8026 (2000).

[15] N. Colonna, M. Hellgren, and S. de Gironcoli, Correlation energy within exact-exchange adiabatic connection fluctuation-dissipation theory: Systematic development and simple approximations, Phys. Rev. B **90**, 125150 (2014).

[16] M. Hellgren and U. von Barth, Linear density response function within the time-dependent exact-exchange approximation, Phys. Rev. B **78**, 115107 (2008).

[17] N. D. Drummond and R. J. Needs, Quantum Monte Carlo study of the ground state of the two-dimensional Fermi fluid, Phys. Rev. B **79**, 085414 (2009).

[18] B. Tanatar and D. M. Ceperley, Ground state of the two-dimensional electron gas, Phys. Rev. B **39**, 5005 (1989).

[19] Within the nuclear physics community, the QBA is often just called RPA, even though it actually contains the exchange term as well. In the language of Ref. [3], our work employs standard RPA, as opposed to self-consistent RPA.

[20] P. Ring and P. Schuck, *The Nuclear Many-Body Problem* (Springer-Verlag, Berlin, 1980).

[21] D. Delion, P. Schuck, and M. Tohyama, Sum-rules and goldstone modes from extended random phase approximation theories in Fermi systems with spontaneously broken symmetries, Eur. Phys. J. B **89**, 45 (2016).

[22] The results discussed in this work do not significantly depend on κ, provided it is small compared to the discretization.

[23] This simply leads to a factor of 2 in front of V_q in Eq. (9c).

[24] The gRPA equation can also be derived in time-dependent mean-field theory [20].

[25] G. Baym, Self-consistent approximations in many-body systems, Phys. Rev. **127**, 1391 (1962).

[26] A. Overhauser, Spin density waves in an electron gas, Phys. Rev. **128**, 1437 (1962).

[27] A. Overhauser, Charge-density waves and isotropic metals, Adv. Phys. **27**, 343 (1978).

[28] H. Kranz, J. Lowenau, and S. Schmitt-Rink, Exchange effects in the static dielectric function and spin susceptibility of the homogeneous electron gas, J. Phys. C **17**, 2121 (1984).

[29] P. Kopietz, *Bosonization of Interacting Fermions in Arbitrary Dimensions* (Springer Science & Business Media, Berlin, 1997), Vol. 48.

[30] H. Zhou, T. Xie, A. Ghazaryan, T. Holder, J. R. Ehrets, E. M. Spanton, T. Taniguchi, K. Watanabe, E. Berg, M. Serbyn, and A. F. Young, Half and quarter metals in rhombohedral trilayer graphene, Nature (London) **598**, 429 (2021).

[31] H. Zhou, L. Holleis, Y. Saito, L. Cohen, W. Huynh, C. L. Patterson, F. Yang, T. Taniguchi, K. Watanabe, and A. F. Young, Isospin magnetism and spin-polarized superconductivity in Bernal bilayer graphene, Science **375**, 774 (2022).

[32] H. Zhou, T. Xie, T. Taniguchi, K. Watanabe, and A. F. Young, Superconductivity in rhombohedral trilayer graphene, Nature (London) **598**, 434 (2021).

[33] N. Morales-Durán, A. H. MacDonald, and P. Potasz, Metal-insulator transition in transition metal dichalcogenide heterobilayer moiré superlattices, Phys. Rev. B **103**, L241110 (2021).

[34] Y. Xu, S. Liu, D. A. Rhodes, K. Watanabe, T. Taniguchi, J. Hone, V. Elser, K. F. Mak, and J. Shan, Correlated insulating states at fractional fillings of moiré superlattices, Nature (London) **587**, 214 (2020).

[35] X. Huang *et al.*, Correlated insulating states at fractional fillings of the WS_2/WSE_2 moiré lattice, Nat. Phys. **17**, 715 (2021).

[36] E. C. Regan *et al.*, Mott and generalized Wigner crystal states in WSE_2/WS_2 moiré superlattices, Nature (London) **579**, 359 (2020).

[37] M. Matty and E.-A. Kim, Melting of generalized Wigner crystals in transition metal dichalcogenide heterobilayer moiré systems, Nat. Commun. **13**, 7098 (2022).

[38] Y. Zhou *et al.*, Bilayer Wigner crystals in a transition metal dichalcogenide heterostructure, Nature (London) **595**, 48 (2021).